Accurate Relative Motion Compensation for Digital Beamforming in Airborne SAR

Juan Pablo Navarro Castillo[a], Marc Jäger[a], Rolf Scheiber[a], and Alberto Moreira[a]
[a]German Aerospace Center (DLR), Microwaves and Radar Institute, Münchener Str. 20, 82334 Oberpfaffenhofen

Abstract

High-resolution wide swath (HRWS) operational modes for spaceborne synthetic aperture radar (SAR) missions are supported by airborne SAR experiments to demonstrate the performance of digital beamforming (DBF) techniques. In practice, the inter-channel motion inconsistencies in airborne DBFSAR must be corrected before azimuth reconstruction occurs. Current motion compensation (MoCo) algorithms can compensate for these inconsistencies but are limited when the dataset is undersampled, as in the case of SAR systems with multiple azimuth phase centers. The innovative solution presented in this paper exploits the fundamentals of multi-channel azimuth reconstruction to relax this limitation and applies channel corrections to account for the differences between the transmitter path and the trajectories of the receivers.

1 Introduction

DBF is a well-known solution to overcome the limitations of a traditional monostatic stripmap SAR system to achieve greater resolutions in azimuth while sweeping a wider swath. In the azimuth direction, the use of techniques based on a multiple azimuth phase center sampling (MAPS) has shown great potential to improve the azimuth resolution even if the operational pulse repetition frequency (PRF) is lower than the bandwidth of the 3dB azimuth antenna pattern [1]. After sending a chirp signal, these systems use several apertures displaced alongtrack to receive the respective echoes. After digitalization, the information of the channels is processed by a multichannel reconstruction algorithm to obtain a resampled SAR signal with an increased equivalent PRF. By doing so, an azimuth ambiguity-free SAR image can be obtained after azimuth reconstruction and focusing, even when working with subsampled and hence ambiguous information in each individual channel.

In the last decades, different reconstruction algorithms have been developed. One of the most widely used solutions is the matrix inversion-based method, which was first proposed in [1]. This algorithm uses the generalized sampling theorem to implement a bank of filters which are built by solving a system of linear equations based on the multi-channel SAR impulse response function (IRF). By adding the range-compressed aliased channels coherently after being processed by the reconstruction filters the approach obtains a resampled output signal with an N times bigger PRF than the operational one, where N is the number of processed channels. Importantly, MAPS reconstruction algorithms cannot perform properly if inter-channel motion inconsistencies are not properly taken into account while implementing the processing chain [2]. Most of the works that study multi-channel azimuth reconstruction algorithms consider these errors to be negligible for spaceborne SAR. Consequently, they do not further investigate these effects. The study introduced in [2] proposes to use a one-step MoCo in collaboration with an aperture-dependent MoCo for multi-channel airborne SAR. However, the aperture-dependent MoCo cannot be used when the individual channels are subsampled. In addition, velocity variations in the azimuth direction are another kind of perturbation that may introduce errors in the reconstruction process. In [3] it was concluded that velocity variations in multi-channel spaceborne SAR can be neglected. Nonetheless, the magnitude and time variance of the average velocity, baselines, and ranges in multi-channel airborne SAR are significantly different than in spaceborne systems. Therefore, these effects need to be considered in the process in order to maximize the performance of the reconstruction. To minimize the impact of the velocity variation, [4] proposes the use of sub-apertures in the reconstruction process. This solution was proposed for reconstruction algorithms based on adaptive methods, which is an alternative to matrix inversion methods.

This paper proposes a new reconstruction approach by extending the conventional multi-channel reconstruction algorithm presented in [1] with three additional processing steps. First, a one-step beam-center MoCo technique is applied before reconstruction. This technique differs from [2], since in the work presented in the coming sections a non-linear reference track is used, leading to smaller residual errors, as explained in more detail in Section 3. Secondly, a residual MoCo correction factor is introduced in the calculation of the reconstruction filters to account for the echoes coming from squint angles different than the center of the beam. Finally, the concept of using sub-apertures to minimize the impact of the velocity perturbation was implemented for the matrix inversion method used throughout this study.

This paper is organized as follows: Section 2 introduces the airborne SAR system used in the experiments and the

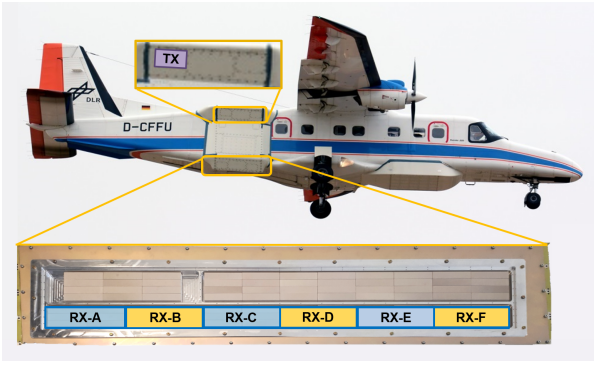

Figure 1 DLR DO 228-212 aircraft showing the location of the antennas. The yellow rectangles correspond to the receiving antennas used for this demonstration.

Parameter	Value
Carrier frequency	9.50 GHz
Chirp bandwidth	400.00 MHz
Range sampling frequency	500.00 MHz
Average sensor altitude	3050.00 m
Target altitude	768.63 m
Average along-track velocity	90.11 m/s

Table 1 The principle parameters of the DBFSAR experiment used in this investigation.

challenges that the irregular motions bring to the MAPS signal processing. Section 3 presents the updated DBF algorithm, including MoCo and azimuth reconstruction techniques. Then, section 4 explains the experiments and simulations, and shows the respective results. Finally, a conclusion is made in section 5.

2 System Characteristics

For the experiments performed in this research, the airborne DBFSAR system of DLR was used. First, the antenna configuration and some important parameters will be introduced. Afterward, the multi-channel IRF and how irregular motion errors influence its definition is explained.

2.1 Airborne System

In **Figure 1** the antenna configuration used in the experiments is depicted. The transmission antenna is placed in the upper part of the aircraft, approximately 1.75m over the receiving antenna array, which is composed of six channels. From the six receiving antennas, just three were used in this investigation: channels B, D, and F. These channels will be from now on referred to as channels 1, 2, and 3, respectively. The selected channels are almost equidistant in azimuth, such that $b_3 - b_2 \simeq b_2 - b_1 \simeq 0.4$m, where b_i is the azimuth separation between the transmitter and the receiver i (see **Figure 2**). All the antennas are designed to operate in X band. The SAR data acquisition used for this work, and on which the simulations are based, took place in 2020 over the DBFSAR calibration site in Kaufbeuren, Germany. Some of the relevant parameters regarding this

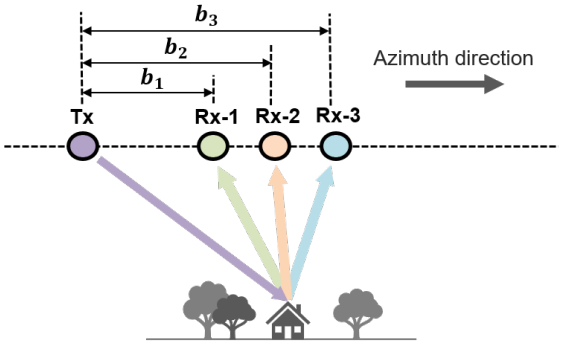

Figure 2 Traditional DBFSAR system based on MAPS operating with three channels displaced in azimuth.

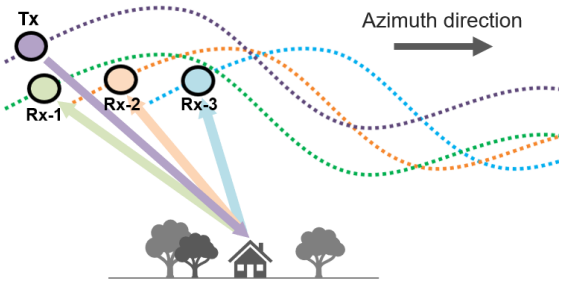

Figure 3 Real DBFSAR system. The three channels are also displaced across-track and in elevation.

flight are listed in **Table 1**. Other important parameters like PRF or azimuth bandwidth will be presented in the results section, as they will be modified from the original values to match the requirements for this experiment.

2.2 Multi-Channel IRF in Airborne SAR

In a DBFSAR system with a single transmitter and multiple receive antennas separated along-track, each channel can be described as a bistatic SAR sensor where the transmitter and receiver are separated by a certain distance in azimuth. This concept is shown in **Figure 2**. Then, [1] defines the multi-channel IRF for a specific channel i in the Doppler domain as:

$$H_i(f,r) = M(f,r) \cdot \exp\left[-j \cdot 2\pi \cdot f \cdot \frac{b_i}{2 \cdot v}\right] \cdot \exp\left[-j \cdot \frac{\pi \cdot b_i^2}{2 \cdot \lambda \cdot r}\right] \quad (1)$$

where $M(f,r)$ is the traditional SAR IRF of a monostatic system with the same spatial sampling as the transmitter. r denotes the slant range and $f \in \left[f_d - \frac{N \cdot PRF}{2}, f_d + \frac{N \cdot PRF}{2}\right]$ is the Doppler frequency, where N and f_d represent the number of channels and frequency Doppler centroid (FDC), respectively. λ is the wavelength and v is the velocity along-track. The first exponential component corresponds to a time shift and the second to a constant phase factor due to a slant range offset between the channels [5]. The constant phase offset is an approximation and does not hold for big baselines, as demonstrated in [6]. For the airborne case described in this paper, the errors coming from

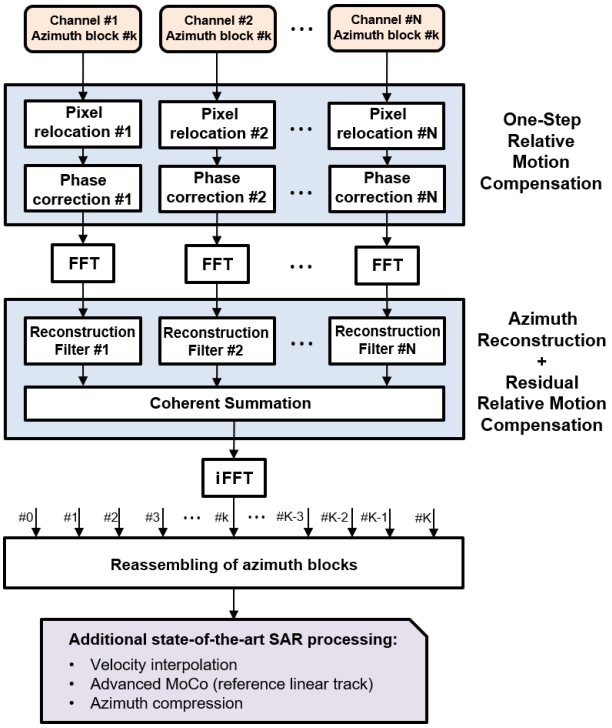

Figure 4 Block diagram of the proposed algorithm.

this assumption are negligible. In real systems (see **Figure 3**) the tracks followed by each aperture are not linear and baselines are present not only in azimuth but also in the other two directions. Furthermore, the platform motion is not linear, and temporally variant attitude angles lead to 3D baselines that change over azimuth. In addition, the along-track velocity is not constant. Consequently, (1) does not hold anymore. For this reason, some modifications and additions need to be done in the traditional MAPS processing chain to account for these effects.

3 The Algorithm

The structure of the reconstruction algorithm based on MAPS proposed in this paper is depicted in **Figure 4**. The key processing steps can be divided into two main groups. The first one is the one-step beam-center MoCo technique and the second one is the azimuth reconstruction including a new residual MoCo correction in the reconstruction filters. Both steps use a bistatic geometry based on a track relocation for each channel to define the respective processing blocks. The channel information is first divided into azimuth blocks or digital sub-apertures, applying a certain overlap between blocks. The azimuth baselines and the velocity along the track are recalculated for each azimuth block. After the reconstruction, all the blocks are reassembled together. Finally, the reconstructed range-compressed image is processed as a normal monostatic SAR image, including advanced MoCo techniques [7].

3.1 Relocation of the Bistatic Tracks

The track corrections applied for each channel are illustrated in **Figure 5**. The aim is to modify the location

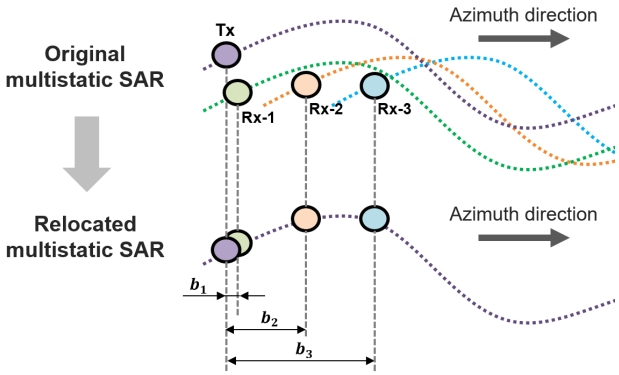

Figure 5 Relocation of Rx antenna tracks to minimize phase errors for the chosen multi-channel IRF.

of the samples in space so that the multi-channel IRF of each channel gets closer to (1). The relocation leaves the azimuth coordinates of the reception (Rx) antenna tracks unaltered and modifies the across-track and elevation so that the Rx antenna tracks follow the path of the transmitter. The motivation for leaving the transmit-track untouched is twofold: First, it is desirable to keep the correction as small as possible such that the reconstruction process does not become dependent on an accurate DEM. Secondly, performing motion compensation onto a non-linear track avoids making strong assumptions regarding the acquisition geometry (e.g., the reconstruction can be applied to circular SAR acquisitions). With this, the goal is to minimize residual phase errors due to a mismatch between DEM and real topography. It should be noted that in contrast to the illustration in **Figure 2**, the samples are not aligned in azimuth as there are also baselines in across-track and elevation. The reason is that, as explained in [5], in the approximation to obtain (1) the range history of the receivers is assumed to be a delayed version of the transmitter range history. If the transmit antenna track is not linear, the only way to match this condition is to interpolate the Rx antenna track onto the transmit antenna track (see **Figure 5**).

3.2 One-Step Relative MoCo

Assuming, for convenience and computational efficiency, that the scene topography can be approximated by a flat surface, the line-of-sight (LOS) distance between each point on the ground and the original and relocated Rx antenna tracks (see **Figure 5**) can be estimated. In this case, the LOS squint angle is the same as the one established by the center of the antenna beam. Then, the range differences between original and relocated tracks for a certain channel i can be defined as:

$$\Delta R_{Rx_i,k}(t_a, r; f = f_d) = R_{Rx_i,k}(t_a, r; f = f_d) - R'_{Rx_i,k}(t_a, r; f = f_d) \quad (2)$$

where $R_{Rx_i}(t_a, r)$ is the LOS distance between the position of the original track and the point on the ground varying over slow time (t_a) and slant range. $R'_{Rx_i}(t_a, r)$ is the

same but for the relocated Rx antenna track. The index k is there to denote that these values are different for each azimuth block. The MoCo correction factor is then calculated as follows:

$$q_{i,k}(t_a, r) = \exp\left[j \cdot \frac{2\pi}{\lambda} \cdot \Delta R_{Rx_i,k}(t_a, r; f = f_d)\right]. \quad (3)$$

Then, supposing a subsampled range-compressed 2D dataset $x_{i,k}(t_a, r)$, the beam-center corrected data can be defined as:

$$\hat{x}_{i,k}(t_a, r) = \tilde{x}_{i,k}(t_a, r) \cdot q_{i,k}(t_a, r) \quad (4)$$

where

$$\tilde{x}_{i,k}(t_a, r) = x_{i,k}(t_a, r + \frac{\Delta R_{Rx_i,k}(t_a, r; f = f_d)}{2}). \quad (5)$$

Since the phase correction is range-dependent, an interpolation of the channel data needs to be performed before this correction happens, as expressed in (5). $\hat{x}_{i,k}(t_a, r)$ will be then transformed in the range-Doppler domain ($\hat{X}_i(f, r)$) and processed by the reconstruction filter. This MoCo technique is called relative MoCo (RelMoCo) because it is a relative correction between two non-linear, bi-static acquisition geometries. Additionally, the RelMoCo is an intermediate MoCo step that just performs small corrections and leaves the output track as non-linear. As shown in **Figure 4**, after signal reconstruction, there is another MoCo process as part of the stripmap SAR image formation workflow, where the major corrections are performed. In this case, it is based on state-of-the-art MoCo techniques that expect an unambiguous azimuth spectrum, which can be achieved after azimuth reconstruction [7].

3.3 Enhanced Azimuth Reconstruction

The one-step RelMoCo is beam-center and therefore it does not take echoes coming from different squint angles into account. This introduces residual errors in the Doppler domain and should be addressed. Current MoCo techniques can correct these errors but they assume a non-aliased spectrum. However, this is not the case in DBF systems based on MAPS, which have an operative PRF lower than the azimuth bandwidth. The proposed solution to this problem is to include the expected residual phase errors after the RelMoCo in the definition of (1). The expression to define the correction factor for the RelMoCo residual phase error is similar to (3), but takes a few new considerations. Now, the LOS range differences will be calculated by varying the squint angle, or in other words, varying the Doppler frequency $f \in \left[f_d - \frac{N \cdot PRF}{2}, f_d + \frac{N \cdot PRF}{2}\right]$. Furthermore, these calculations must be done for a fixed time instant, since in the Doppler domain there is no azimuth spatial resolution. As it is expected to work with azimuth blocks or sub-apertures (see **Figure 4**), the fixed time instant t_0 was set to match the middle azimuth sample of each block. Then, the new LOS range differences can be defined as:

$$\Delta R_{Rx_i,k}(f, r; t_a = t_0) = R_{Rx_i,k}(f, r; t_a = t_0) - R'_{Rx_i,k}(f, r; t_a = t_0). \quad (6)$$

The last remark before defining the residual RelMoCo factor is that it is expected that the dataset was already processed by a RelMoCo filter in the azimuth-range domain, as expressed in (4). Consequently, LOS differences used in the one-step beam-center RelMoCo factor must be subtracted from the new LOS range differences. Gathering all this information, the residual RelMoCo correction factor can be expressed as:

$$\Delta q_{i,k}(f, r) = \exp\left[j \cdot \frac{2\pi}{\lambda} \cdot \Delta S_{i,k}(f, r)\right] \quad (7)$$

and

$$\Delta S_{i,k}(f, r) = \Delta R_{Rx_i,k}(f, r; t_a = t_0) - \Delta R_{Rx_i,k}(r; f = f_d, t_a = t_0) \quad (8)$$

where $\Delta R_{Rx_i,k}(r; f = f_d, t_a = t_0)$ denotes the LOS range differences calculated for the one-step RelMoCo for the time instant $t_a = t_0$. Obviously, this is an approximation as it assumes that the variation over slow time of the RelMoCo correction is negligible, which may not be true for large blocks. Therefore, it is recommended to keep the size of the azimuth blocks as small as possible, while ensuring that the resolution in the Doppler domain is high enough.

The factor calculated in (7) cannot be applied in the same way as shown in (4), since the Doppler spectrum is aliased. However seeing the problem from another perspective, the residual RelMoCo component can be included in (1) as part of the multi-channel IRF. Then, the new IRF can be expressed as

$$G_{i,k}(f, r) = M_k(f, r) \cdot \Delta q^*_{i,k}(f, r) \cdot \exp\left[-j \cdot 2\pi \cdot f \cdot \frac{b_{i,k}}{2 \cdot v_k}\right] \cdot \exp\left[-j \cdot \frac{\pi \cdot b^2_{i,k}}{2 \cdot \lambda \cdot r}\right] \quad (9)$$

where the residual RelMoCo error is defined as the conjugated of the correction factor introduced in (7). As shown in [1], what the azimuth reconstruction does is not just remove the azimuth ambiguities, but also remove the channel-dependent components which are defined in the multi-channel IRF. The only components in the multi-channel IRF that are kept after the reconstruction are the ones that are common among the channels. In the case of the IRF defined in (9), the only common factor along the channels is $M_k(f, r)$ which is the traditional monostatic IRF for the azimuth block k. Returning to the residual motion error, this means that including (7) in (1) as an additional channel-dependent component will remove the residual motion errors once the reconstruction process is done. With the proposed additional processing steps, the standard approach for multi-channel reconstruction presented in [1] can be applied.

4 Experimental Setup and Results

4.1 Point Target Simulation

As an initial test of the proposed algorithm, a point target was simulated with the configuration described in **Table 1**.

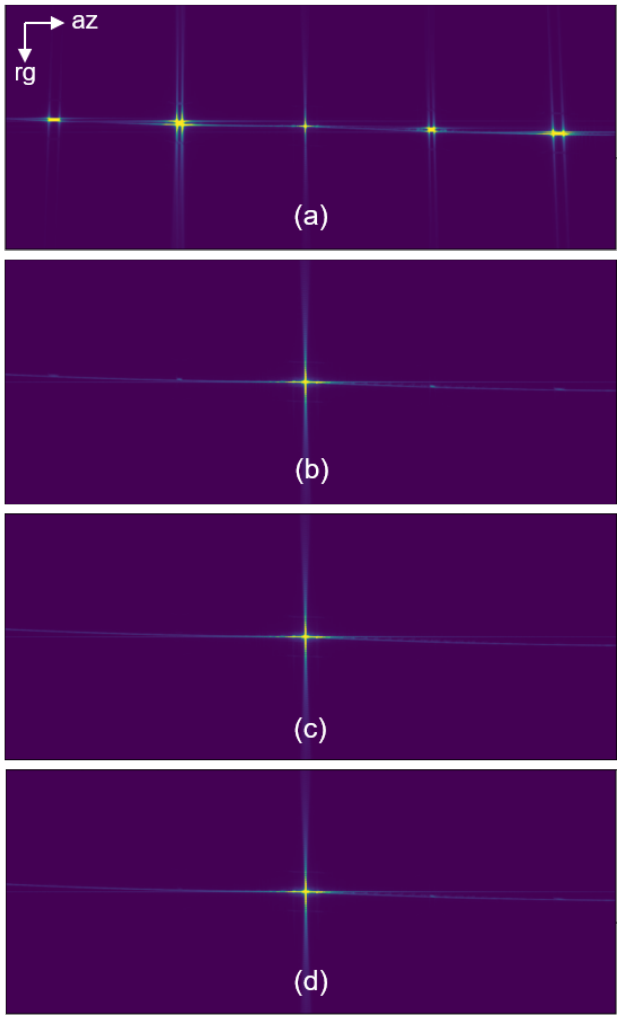

Figure 6 (a) Point target focused in azimuth after being processed with different reconstruction configurations: azimuth blocks and no RelMoCo, (b) azimuth blocks and just one-step RelMoCo, (c) full RelMoCo with azimuth blocks, and (d) full RelMoCo without blocks. The horizontal and vertical axis correspond to azimuth and range, respectively.

	Case a	**Case b**	**Case c**	**Case d**
$AASR_p$	-8.7dB	-56.6dB	-63.2dB	-58.9dB
$AASR_i$	5.5dB	-44.3dB	-52.9dB	-48.2dB

Table 2 Highest AASR for each case in the simulation.

The position and characteristics of the point target were taken from an actual point target in the real experiment. For this simulation, the antenna setup presented in **Section 2** was used. The three bistatic tracks were the same as in the original flight. However, the individual channel antenna patterns were set to be identical and isotropic. The operative PRF was 150 Hz with an azimuth bandwidth of 400 Hz, assuring that the individual channels were subsampled. The azimuth sample spacing of the multi-channel system was close to uniform. Four different setups for the reconstruction algorithm were evaluated. For the first three scenarios blocks with a total of 128 azimuth samples

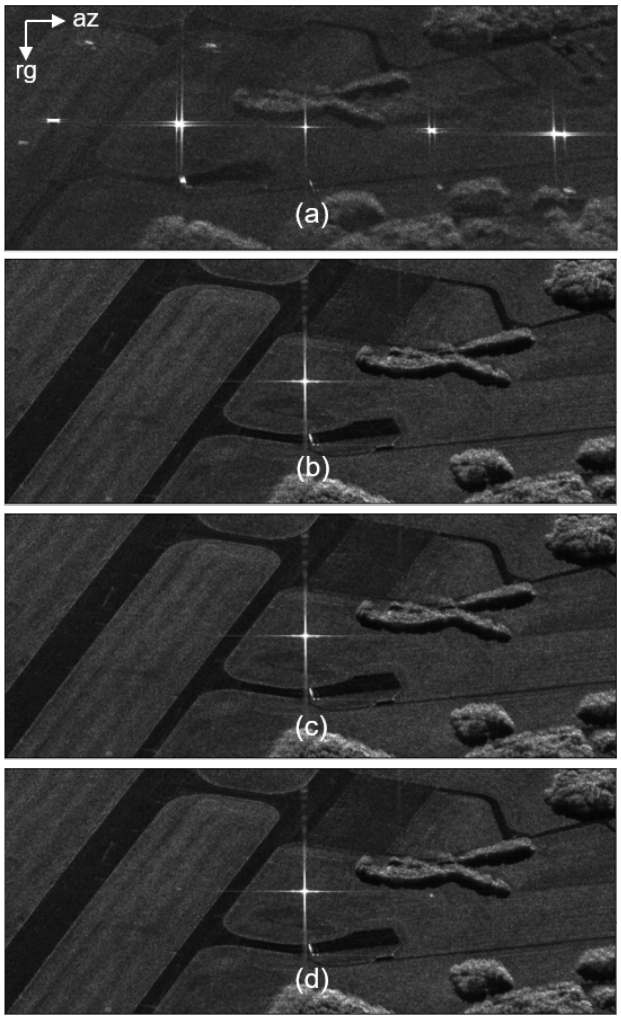

Figure 7 Real point target focused in azimuth after being processed with different configurations. The cases are the same as in **Figure 6**.

	Case a	**Case b**	**Case c**	**Case d**
$AASR_p$	-11.7dB	-51.4dB	-52.5dB	-47.3dB
$AASR_i$	4.5dB	-39.5dB	-41.3dB	-36.1dB

Table 3 Highest AASR for each case in the real scene.

were used. The first reconstruction did not include any RelMoCo, and the second included the one-step RelMoCo but no residual RelMoCo. Finally, the third and fourth reconstructions included all processing steps described in **Section 3**. However, the fourth reconstruction did not include block processing in azimuth. The 2D point target response after SAR image formation is applied to the reconstruction result for each scenario is depicted in **Figure 6**. The results are summarized in **Table 2**. The performance was evaluated using the azimuth ambiguity-to-signal ratio (AASR), analyzing both the peak powers ($AASR_p$) and the integrated powers ($AASR_i$).

It is clear that not applying any motion correction before reconstruction prevents a proper suppression of the azimuth ambiguities. One can also see that by just applying the one-step RelMoCo the performance of the reconstruc-

tion is considerably better than in the previous case. Nevertheless, this could change if wider azimuth bandwidths are processed since this will increase the residual errors in the borders of the spectrum. Then, the residual RelMoCo using azimuth block processing further improves the ambiguity suppression, achieving the best AASR among the four cases. In addition, working with blocks allows the implementation of parallel processing, which reduces the processing time considerably.

4.2 Real Data

In the real experiment, the operative PRF was 3000 Hz and the azimuth bandwidth was approximately 600 Hz. To generate a similar scenario as the one studied in the simulation, some pre-processing steps needed to be conducted. First, the undesired effects coming from the antenna patterns were corrected in each channel before applying a decimation to the range-compressed azimuth blocks. Then, the corrected signal was low-pass filtered in the Doppler domain to reduce the bandwidth to 400 Hz. Finally, the signal was decimated in azimuth with a decimation factor of 20 to obtain a PRF of 150 Hz and create aliased input data. At this point, the setup for the experiment with real data was considered equivalent to the simulation. The real results of SAR image formation applied to the results of reconstruction, which include natural targets as well as the simulated point targets, are depicted in **Figure 7**. Then, **Table 3** shows the corresponding AASR, derived from the point target responses. As observed in the simulations, the combination of a one-step RelMoCo with a residual RelMoCo showed an outstanding performance concerning ambiguity suppression. In case (a) in **Figure 7**, the scene seems to be shifted in comparison with the rest of images. This effect can be explained observing the values of the integrated AASR in **Table 3**. For case (a) the AASR is positive, meaning that the integrated power of the ambiguity is bigger than the integrated power of the target.

Several important aspects must be further evaluated to improve the robustness of the algorithm. For instance, it is important to study the impact of non-uniform azimuth sampling on noise scaling, which is a well-known drawback in matrix inversion-based reconstructions. Apart from that, when the channel baselines get bigger, the constant phase component approximation in the multi-channel IRF does not hold. This needs to be considered if the algorithm is used for multi-static spaceborne systems. Additionally, the technique can be extended to DBF systems based on MAPS with different antenna patterns for each receiving channel by generalizing the definition of the multi-channel IRF presented in (9). Finally, the sensitivity of the reconstruction to height mismatches concerning the flat DEM must be investigated.

5 Conclusions

This paper has presented an innovative method to deal with inter-channel motion inconsistencies in airborne DBFSAR systems operating with a PRF lower than the azimuth bandwidth. The idea of exploiting the definition of the multi-channel IRF to correct residual motion errors in the Doppler domain has further improved the suppression of azimuth ambiguities after reconstruction and SAR image formation. Moreover, it was demonstrated that it is not required to impose perfect linear tracks to perform a proper signal reconstruction. Using the relocation of the Rx antenna tracks to follow the same non-linear path as the transmitter has shown great potential even in cases where a real DEM of the scene is not available. Finally, the use of subapertures minimizes the impact of velocity variations, facilitates the residual RelMoCo, and can also be used to reduce and optimize the total processing time.

Several scenarios will be further studied to improve the robustness of the presented algorithm, including challenging scenarios with bigger azimuth baselines, different antenna patterns, strong non-uniform sampling, or strong topographic variability within the scene. In summary, the reconstruction algorithm based on RelMoCo has proven very effective at removing undesired azimuth ambiguities and will be further investigated in future studies.

6 Literature

[1] G. Krieger, N. Gebert, and A. Moreira, "Unambiguous SAR Signal Reconstruction From Nonuniform Displaced Phase Center Sampling," *IEEE GRSL*, vol. 1, no. 4, pp. 260–264, Oct. 2004.

[2] Z. Chen, Z. Zhang, J. Qiu, Y. Zhou, W. Wang, H. Fan, and R. Wang, "A Novel Motion Compensation Scheme for 2-D Multichannel SAR Systems With Quaternion Posture Calculation," *IEEE TGRS*, vol. 59, no. 11, pp. 9350–9360, Nov. 2021.

[3] N. Sakar, M. Rodriguez-Cassola, P. Prats-Iraola, and A. Moreira, "Azimuth Reconstruction Algorithm for Multistatic SAR Formations With Large Along-Track Baselines," *IEEE TGRS*, vol. 58, no. 3, pp. 1931–1940, Mar. 2020.

[4] S.-X. Zhang, M.-D. Xing, X.-G. Xia, L. Zhang, R. Guo, Y. Liao, and Z. Bao, "Multichannel HRWS SAR Imaging Based on Range-Variant Channel Calibration and Multi-Doppler-Direction Restriction Ambiguity Suppression," *IEEE TGRS*, vol. 52, no. 7, pp. 4306–4327, Jul. 2014.

[5] N. Gebert, G. Krieger, and A. Moreira, "Digital Beamforming on Receive: Techniques and Optimization Strategies for High-Resolution Wide-Swath SAR Imaging," *IEEE TAES*, vol. 45, no. 2, pp. 564–592, Apr. 2009.

[6] N. Sakar, M. Rodriguez-Cassola, P. Prats-Iraola, A. Reigber, and A. Moreira, "Analysis of Geometrical Approximations in Signal Reconstruction Methods for Multistatic SAR Constellations With Large Along-Track Baseline," *IEEE GRSL*, vol. 15, no. 6, pp. 892–896, Jun. 2018.

[7] P. Prats, K. A. Camara de Macedo, A. Reigber, R. Scheiber, and J. J. Mallorqui, "Comparison of Topography- and Aperture-Dependent Motion Compensation Algorithms for Airborne SAR," *IEEE GRSL*, vol. 4, no. 3, pp. 349–353, Jul. 2007.